Chemical Physics Letters 715 (2019) 84–90

Contents lists available at ScienceDirect

Chemical Physics Letters

journal homepage: www.elsevier.com/locate/cplett

Research paper

The comparative study of new carboxylated 1,3-indanedione sensitizers with standard cyanoacetic acid dyes using co-adsorbents in dye-sensitized solar cells

Hyeonjun Jeong[a], Ramesh Kumar Chitumalla[b], Dong Woo Kim[a], S.V. Prabhakar Vattikuti[a], Suresh Thogiti[a], Rajesh Cheruku[a], Jae Hong Kim[a], Joonkyung Jang[b], Ganesh Koyyada[a,*], Jae Hak Jung[a,*]

[a] Department of Chemical Engineering, Yeungnam University, 214-1, Dae-hakro 280, Gyeongsan, Gyeongbuk 712-749, South Korea
[b] Department of Nanoenergy Engineering, Pusan National University, Busan 46241, South Korea

HIGHLIGHTS

- The synthesized carboxylated 1,3-indanedione dyes DSSC performance were evaluated.
- The carboxylated 1,3-indanedione dyes showed 100 nm red-shifted absorption spectra.
- The IPCE of carboxylated 1,3-indanedione sensitizers have been extended upto 800 nm.
- The reasons for low efficiency of 1,3-indanedione sensitizers were discussed.

ARTICLE INFO

Keywords:
Dye-sensitized solar cells
Co-adsorbents
Organic sensitizer
DFT

ABSTRACT

Two new carboxylated 1,3-indanedione sensitizers (MPhe-ind and BPhe-ind) were synthesized and their dye-sensitized solar cells (DSSC) performance were compared with the corresponding standard cyanoacetic acid sensitizers (MPhe-cn and BPhe-cn). The carboxylated 1,3-indanedione sensitizers have shown almost 100 nm enhanced absorption curves compared to the cyanoacetic acid dyes with an extended IPCE curve up to 800 nm. Despite greater absorption and electrochemical properties, the synthesized dyes showed moderate efficiencies (2.10% and 2.67%) than standard dyes. The low electron injection efficiency and recombination of carboxylated 1,3-indanedione might be responsible for low efficiency. Detailed investigation studies have been performed and complemented with the theoretical studies.

1. Introduction

The past few decades have seen remarkable research efforts dedicated to dye-sensitized solar cells (DSSCs) [1–3] owing to their synthetic and purification ease over the conventional silicon solar cells. The initial DSSC device was reported by ÓRegan and Grätzel [4], since then efforts to develop efficient and stable devices have been taken up by researchers all around the globe. The photosensitizer is one of the crucial components in getting the optimum efficiency, which harvests the solar energy and injects the photogenerated electron into the conduction band of semiconductor oxide [5,6]. Early reports of zinc porphyrin [7,8], ruthenium complexes [9–11] and metal-free organic dyes [12–15] are some of the benchmark sensitizers in DSSCs. The zinc porphyrin-based sensitizers [7] have shown 13% record efficiency in association with the cobalt bipyridine ($[Co(bpy)_3]^{2+/3+}$) based redox electrolyte, whereas ruthenium (II) based dye [9,16,17] have achieved above 11.4% efficiency till date. However, the limitations corresponding to these complexes such as the rare resources of ruthenium and zinc metals, high manufacturing cost; heavy-metal toxicity and environmental problems would avert their widespread applications [18]. To overcome the above issues of metal complexes, the metal-free organic sensitizers have been studied owing to their low cast preparation process, easy structural modifications and high molar extinction coefficient. Moreover, organic dyes as a sensitizer in DSSC have reached 14% efficiency [19] as reported earlier in the literature. Therefore, much concentration has been devoted in the design, modification and

* Corresponding authors. Tel.: +821020266547.
E-mail addresses: ganeshkoyyada@ynu.ac.kr, ganeshkoyyada@gmail.com (G. Koyyada), jhjung@ynu.ac.kr (J.H. Jung).

https://doi.org/10.1016/j.cplett.2018.11.026
Received 17 August 2018; Received in revised form 10 November 2018; Accepted 12 November 2018
Available online 13 November 2018
0009-2614/

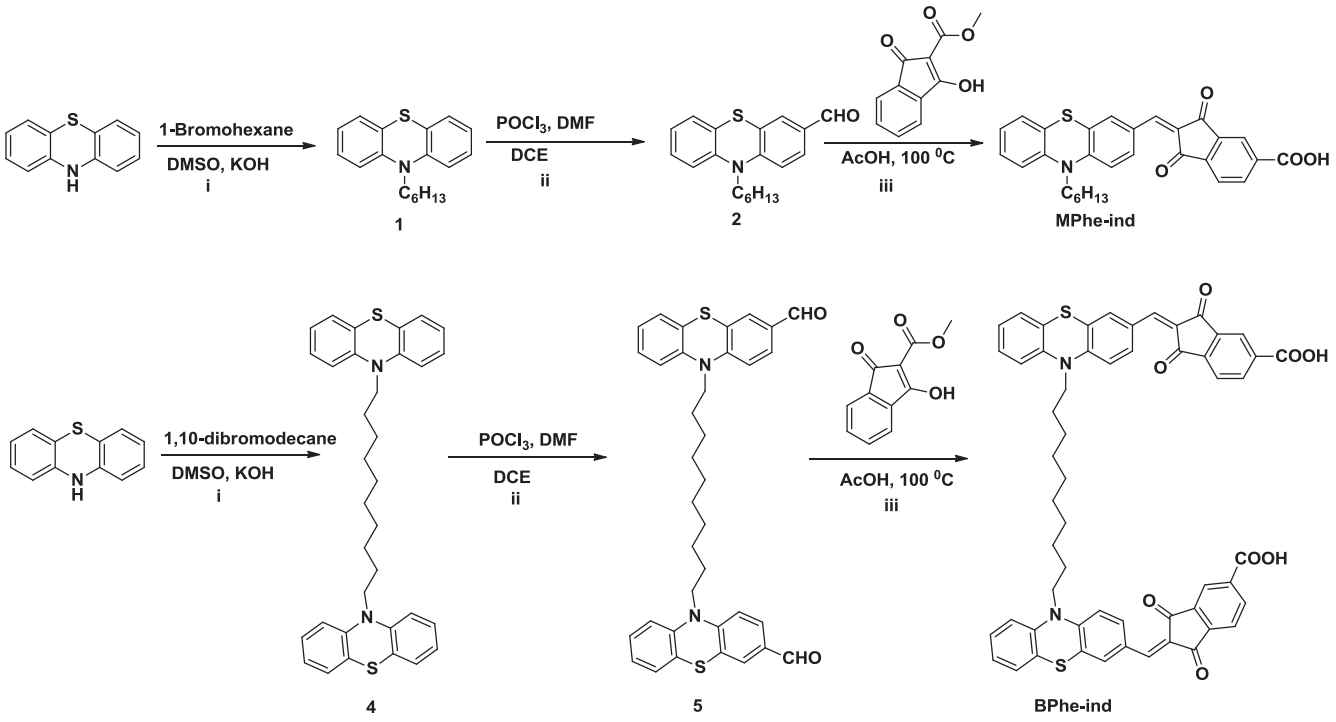

Scheme 1. Synthesis of MPhe-ind and BPhe-ind.

development of new metal-free organic sensitizers as efficient light harvesting materials for DSSCs application [20–22].

Derong Cao et al. [23] presented novel double branched (DB) phenothiazine-based D-π-A mannered organic sensitizer, which showed enhanced efficiency compared to their mono branched D-π-A sensitizers. In recent times, our research group also reported few new double branched organic dyes by structural engineering of the molecule with symmetrical and unsymmetrical anchoring groups with varying alkyl chains [24,25]. Among them, D-A type structural design was attracted more interest owing to their small size and remarkable optical and efficient intramolecular charge transfer (ICT) property [26]. Generally, the D-A type dyes have more tendency to anchoring on the TiO_2 semiconductor. Efficient dye adsorption and its structural configurations are the key factors for improving photovoltaic efficiency [26,27]. Mishra et al. also stated that the performance of the DSSC device is not only subjected to design of the sensitizer and also influenced by its physical properties like morphology and aggregation [18]. The main role of anchoring group of the sensitizer is to bind strongly on semiconductor surface through chemical bond and electron transfer from donor to the semiconductor conduction band. So far the reported cyanoacetic acid anchoring groups have shown good performance, however, the optimization on anchoring group side is rather limited. In this study, the anchoring carboxylated 1,3-indanedione group was examined in D-A construction manner for a better understanding of the effect of anchoring group on the semiconductor.

Numerous organic chromophores such as phenothiazine, triphenylamine, dithiafulvenyl, tetrahydroquinoline, carbazole, indoline have been examined as a donor in organic dyes [28,29]. Among all the above-mentioned chromophores, phenothiazine act as a strong donor and holds a large proportion owing to its unique features like non-planar butterfly conformation, which helps to decrease the dye aggregation and excimer formation. Moreover, the presence of the electron rich sulfur and nitrogen heteroatoms furnish phenothiazine as a strong donor. Keeping all these concepts in view, we herein designed two new organic dyes (Fig. S1) with single and double branched manner along with new anchoring group i.e. carboxylated 1,3-indanedione. In particular, we have examined the acceptance property of carboxylated 1,3-indanedione (**MPhe-ind** and **BPhe-ind)** on mono and double branched patterns because the double branched patterns would inhibit the electron recombination and increase the effective electron transfer into the TiO_2 semiconductor. The aggregation property of these molecules examined with co-adsorbents like chenodeoxycholic acid (CDCA) and palmitic acids (PA) and these DSSCs performances were compared with the corresponding cyanoacetic acid dyes (previously synthesized by our group) [24].

2. Experimental section

2.1. General

The phenothiazine, bromohexane, and dibromhexane starting materials were purchased from Sigma-Aldrich. The solvents and chemicals used for this work were analytical grade and all the reactions in this work were carried out under an argon atmosphere. Chromatographic separations were performed on 60–120 mesh silica gel. ^1H and ^{13}C NMR have acquired on Agilent unity inova Bat (500 MHz) spectrometers and analyzed in $CDCl_3$ or DMSO-d_6 by using tetramethylsilane (TMS) internal standard. UV–Visible absorption spectra were measured on a Cary 5000 UV–Vis-NIR Spectrophotometer. Emission spectra were recorded on a Jobin-Yvon Horiba model fluorolog3 fluorescence spectrometer. The cyclic or deferential pulses voltammograms were recorded in DMF solution contain dye (0.3 mM) and 0.1M tetrabutylammoniumhexafluorophosphate (n-Bu_4NPF_6). The three electrode setup was used for recording, with pt, Pt wire, and Ag/AgCl as the working, counter and reference electrodes with a 100 mV/s scan rate.

3. Result and discussion

The Scheme 1 depicts the synthesis steps of **MPhe-ind** and **BPhe-ind** sensitizers. The commercially accessible phenothiazine and bromo alkanes starting material were subjected to alkylation reaction to afford the compound 1 and 4 with 80–82% yield. Compound 1 and 4 were formylated using $POCl_3$ and DMF to produce the intermediate

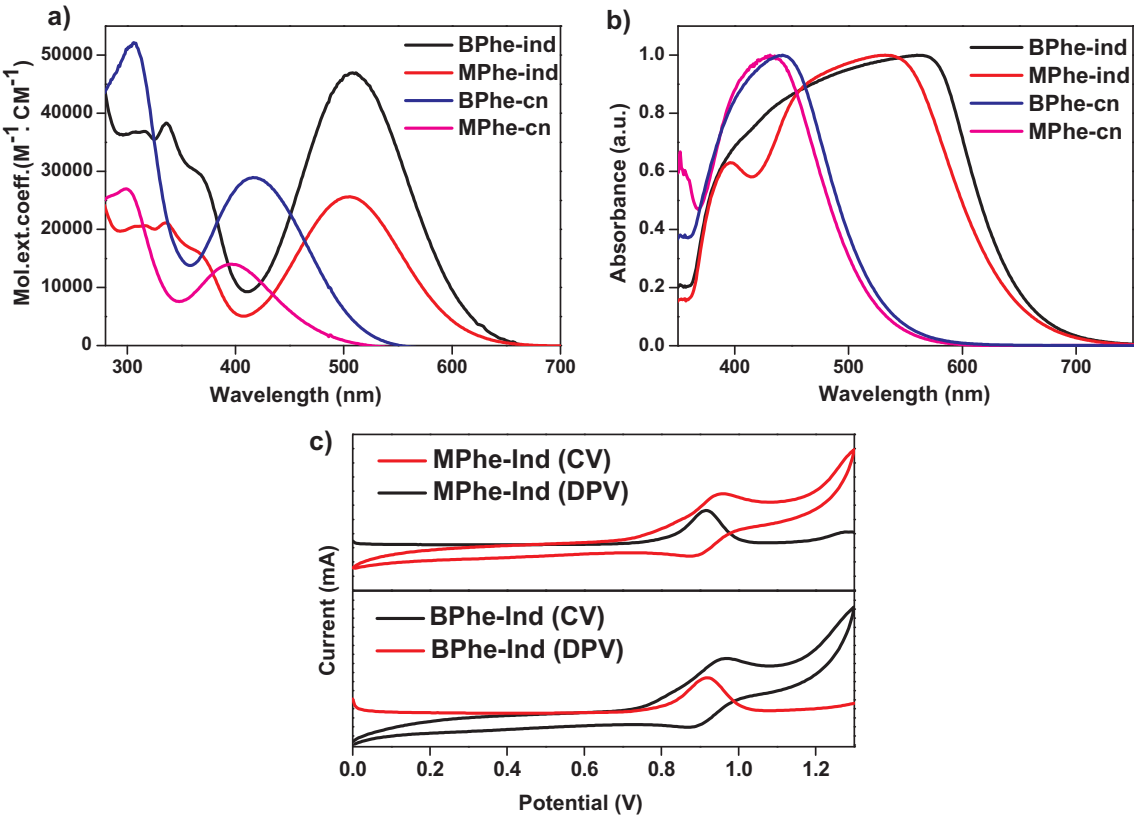

Fig. 1. (a) Comparative UV–Visible spectra of carboxylated 1,3-indanedione dyes and cyanoacetic acid dyes in DMF. (b) UV–Visible absorption spectra of carboxylated 1,3-indanedione dyes and cyanoacetic acid dyes on TiO_2 thin film. (c) Cyclic voltammetry (CV) and differential pulse voltammetry (DPV) of **BPhe-ind** and **MPhe-ind** dyes in DMF.

compound 2 and 5with 74–77% yield. Finally, the desired compounds (**MPhe-ind** and **BPhe-ind**) were accomplished with moderate yields (65%) by condensation with methyl 3-hydroxy-1-oxo-1H-indene-2-carboxylate. Detailed synthesis procedure have been explained in the electronic supporting information (ESI).

3.1. Photophysical and electrochemical properties

The UV–Visible absorption spectra of carboxylated 1,3-indanedione and cyanoacetic acid dyes were measured in DMF as shown in Fig. 1a and the associated data are depicted in Table 1. All the dyes exhibited two distinct bands. The first one *ca.* 250–400 nm is corresponding to the π-π* transition and the later one ca. 400–650 nm is corresponding to the intramolecular charge transfer (ICT). In comparison to the solution state absorption spectra of cyanoacetic acid dyes and the synthesized carboxylated 1,3-indanedione dyes (Fig. 1a), the synthesized **BPhe-ind** and **MPhe-ind** dyes have shown high λ_{max} i.e. 507 and 504 nm with extended absorption curve up to 650 nm. On the other hand cyanoacetic acid dyes have shown 397 and 416 nm λ_{max} and the absorption curve was extended up to 550 nm. It indicates the strong electron withdrawing ability of carboxylated 1,3-indanedione group over cyanoacetic acid [26]. Among, the four dyes, all most double the molar extinction coefficient was observed for **BPhe-ind** ($0.4 \times 10^5\,M^{-1}\,cm^{-1}$) and **BPhe-cn** ($0.29 \times 10^5\,M^{-1}\,cm^{-1}$) than their corresponding monomers **MPhe-ind** ($0.25 \times 10^5\,M^{-1}\,cm^{-1}$) and **MPhe-cn** ($0.14 \times 10^5\,M^{-1}\,cm^{-1}$). Double the number of units in dimers (**BPhe-ind and MPhe-cn)** might be responsible for double the molar extinction coefficient. Fig. 1b displays the absorption spectra of carboxylated 1,3-indanedione dyes and cyanoacetic acid dyes on TiO_2 film. Surprisingly, the absorption curves of **MPhe-ind** and **BPhe-ind** dyes on TiO_2 have shown a bathochromic shift of 40 and 70 nm, relative to their solution state absorption spectra and these absorption curves was extended up to 750 nm. The enhanced absorption properties of dyes might be attributed to the J-aggregation on the TiO_2 surface [30].

Table 1
Optical and electrochemical data of **MPhe-ind** and **BPhe-ind** dyes.

Dye	λ_{abs}(nm)[a] (solution)	$\varepsilon(M^{-1}\,cm^{-1})$	λ_{abs}(nm)[b] (TiO_2)	λ_{em}(nm)[c]	E_{0X} (V)[d]	$E_{0\text{-}0}$ (V)[e]	E_{0X}^*(V)[f]
MPhe-ind	504	25,483	546	756	0.923 V	2.04	−1.117
BPhe-ind	508	46,749	572	765	0.929	2.02	−1.091
MPhe-cn	397	14,345	430	543	0.902	2.54	−1.638
BPhe-cn	416	29,075	441	644	0.913	2.43	−1.517

[a] Absorption spectra were measured in DMF.
[b] Absorption spectra were measured on TiO_2 thin film.
[c] Emission spectra were measured in DMF.
[d] Oxidation potentials were recorded by CV and DPV.
[e] The band gap, $E_{0\text{-}0}$, was calculated from the absorption and emission intercept plots.
[f] E_{OX}^* were derived by subtracting $E_{0\text{-}0}$ from E_{OX}.

Further, the Stokes shift values calculated from absorption emission intercepts of **MPhe-ind** and **BPhe-ind** dyes are 252 nm and 257 nm, which indicate the excellent ICT between the donor and acceptor.

Differential pulse voltammetry (DPV) and cyclic voltammetry (CV) experiments were performed to determine the energy levels i.e. ground state oxidation potential (GSOP) and excited state oxidation potentials (ESOP) of the carboxylated 1,3-indanedione dyes and cyanoacetic acid dyes (Fig. S3). Fig. 1c represents the oxidation potentials of **MPhe-ind** and **BPhe-ind** dyes, these experiments were employed in DMF solution containing 0.1 M n-Bu_4NPF_6 supporting electrolyte and the corresponding data have been depicted in Table 1. The measured oxidation potential values (GSOP) of **MPhe-ind** and **BPhe-ind** dyes are 0.923 V and 0.929 V (vs. SHE) respectively, which are sufficiently more positive than that of I^-/I_3^- redox potential (~0.4 V vs SHE) thereby helping in effective dye regeneration. The ESOP (E_{OX}^*) of **MPhe-ind** and **BPhe-ind** derived from E_{OX}-$E_{0\text{-}0}$ formula are −1.11 and −1.09 V vs SHE, respectively, where $E_{0\text{-}0}$ was determined from the intercept of fluorescence and absorption curves (Fig. S2a and b). ESOP (E_{OX}^*) of **MPhe-ind** and **BPhe-ind** are more negative than the conduction band potential of TiO_2, which ensures enough driving force for the proficient electron injection processes [31].

3.2. Computational studies

To explore the effect of carboxylated 1,3-indanedione anchoring group on DSSC photovoltaic performance over the cyanoacetic acid, the simulated optical, electrochemical, and adsorption properties of **MPhe-ind** and **BPhe-ind** dyes have been analyzed using Gaussian 09 quantum chemical program and compared with cyanoacetic acid dyes properties [32]. The structural geometry optimization of all the dyes was carried out by employing B3LYP functional [33–35] in combination with the 6-31G(d) basis set and presented in Figs. 2 and S5. The optical, electrochemical properties and molecular orbital transitions of the dyes were obtained by employing TDDFT formalism with PBE0 [36,37] hybrid functional and 6-31G(d) basis set. We have calculated the first 25 singlet-singlet excitations to simulate the absorption spectra.

The optimized geometries and the electron density distribution in frontier molecular orbitals of carboxylated 1,3-indanedione dyes are presented in Fig. 2 and the cyanoacetic acid based dyes are shown in Fig. S5. It is obvious and found from optimized geometry that the phenothiazine existed as non-planar butterfly structure in all the dyes. The study about the electron density distribution in frontier molecular orbitals of HOMO and LUMO states was helpful to understand the charge transfer phenomena from Fig. 4. The electron density in HOMO state is mainly located over phenothiazine (donor) and is shifted to the carboxylated 1,3-indanedione group in LUMO. The comparable electron distributions of LUMO frontier molecular orbitals of carboxylated 1,3-indanedione and cyanoacetic acid based dyes are presented as 3d graphical manner (Fig. 4). The calculated electron density on −COOH group in LUMOs of **MPhe-ind** and **BPhe-ind** are 5.6 and 5.3%, respectively, while **MPhe-cn** and **BPhe-cn** have 14.6 and 14.5%, respectively. The low electron density on −COOH group of LUMOs in **MPhe-ind** and **BPhe-ind** dyes is due to the presence of two carbonyl groups on the carboxylated 1,3-indanedione group, which involved in conjugation with donor molecule, as a result, the extent of electron reaches to the carboxyl group is decreased. The low electron density on −COOH group in LUMO state indicates the low electron injection into the TiO_2 conduction band, probably it might be the reason for low DSSCs efficiencies of **MPhe-ind** and **BPhe-ind** dyes over **MPhe-cn** and **BPhe-cn**.

The theoretically simulated absorption spectra of **MPhe-ind** and **BPhe-ind** are depicted in Fig. 4 and absorption data are compiled in Table 2. To mimic the experimental solvent conditions, we used polarizable continuum model [38,39] in the TDDFT simulations to define the DMF solvent. The theoretical absorption maxima are 514 and 536 nm for **MPhe-ind** and **BPhe-ind**, respectively. The theoretical

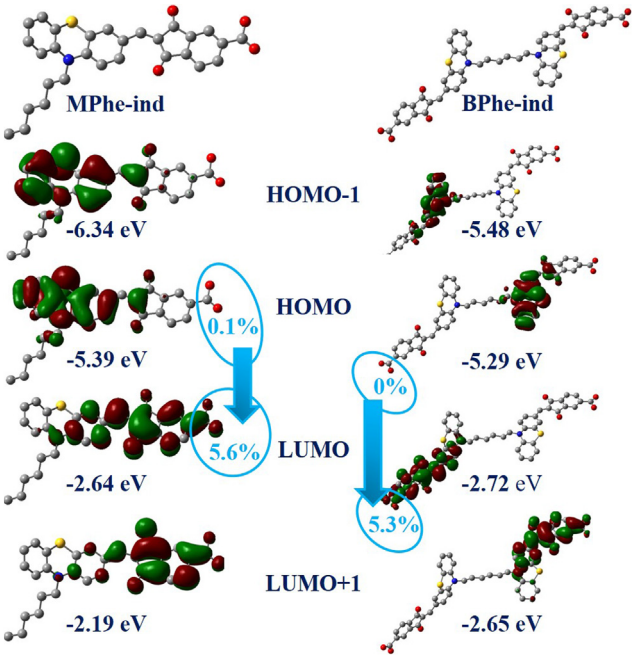

Fig. 2. Optimized geometries and electron density distribution of **MPhe-ind** and **BPhe-ind**. The percentage contribution of the molecular orbital density on anchoring group is shown as encircled part. The Kohn-Sham eigenvalues are given in eV.

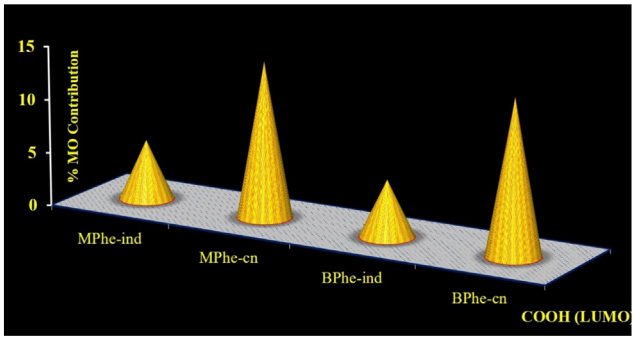

Fig. 3. Comparative electron density contribution of anchoring group in LUMO, MPhe-ind versus MPhe-cn and BPhe-ind versus BPhe-cn.

absorption maximum of **MPhe-ind** (514 nm) is in excellent agreement with that of the experiment (504 nm). Though the theoretical absorption maximum of **BPhe-ind** (536 nm) is slightly over estimated with that of experiment (508 nm), the trend i.e., redshifted absorption has been achieved from **MPhe-ind** to **BPhe-ind**. The first two transitions of BPhe-ind dye occurring at 536 and 515 nm which are corresponding to the excitations of HOMO → LUMO + 1 and HOMO-1 → LUMO, respectively. In both the transitions, the intramolecular charge transfer is on same **MPhe-ind** unit within the **BPhe-ind** dye.

As the interaction between dye and TiO_2 plays a vital role in deciding the device performance, we have carried out the adsorption studies of **MPhe-ind** and **MPhe-cn** on a $(TiO_2)_{16}$ cluster (Fig. 5). The chosen $(TiO_2)_{16}$ is reported to simulate and predict the electronic properties of experimental TiO_2 results [40]. The adsorption studies of **MPhe-ind** and **MPhe-cn** on TiO_2 were performed to evaluate the effect of anchoring group (carboxylated 1,3-indanedione vs. cyanoacetic acid) on overall power conversion efficiency. First, the isolated dyes were optimized and later adsorbed on pre-optimized TiO_2 in a bidentate bridging mode, then optimized the dye adsorbed TiO_2. The adsorption is dissociative i.e., the hydrogen atom of the anchoring −COOH group is transferred to the TiO_2 surface. The adsorption energy is calculated by

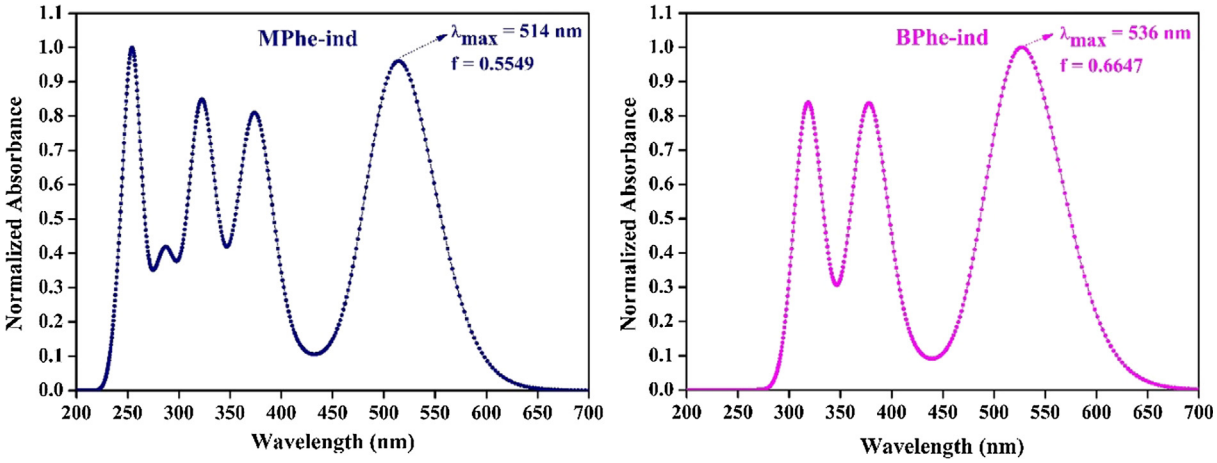

Fig. 4. Simulated UV–visible absorption spectra of the **MPhe-ind** and **BPhe-ind** obtained at TD-PBE0/6-31G(d) level of theory in DMF solvent.

subtracting the energy of the total system from the sum of the energies of the dye and TiO_2:

$$E_{ads} = (E_{Dye} + E_{TiO_2}) - E_{Dye@TiO_2}$$

The calculated adsorption energies of **MPhe-ind** and **MPhe-cn** are 2.42 and 11.91 kcal/mol, respectively. The low adsorption energy obtained for **MPhe-ind** is responsible for the low J_{SC} and thereby low efficiency.

3.3. Photovoltaic properties

The newly synthesized carboxylated 1,3-indanedione dyes were evaluated for DSSCs with and without co-adsorbents such as CDCA or PA and these photovoltaic performances were compared with the cyanoacetic acid based dyes under the similar experimental conditions. All these dyes DSSCs photovoltaic device performances were examined using the 0.25 cm^2 active area of TiO_2 electrode by thermally stable redox shuttle containing 0.5 M 1,2-dimethyl-3-propylimidazole iodide (DMPII), 0.05 M I_2 and 0.1 M LiI in acetonitrile. The obtained photocurrent-voltage curves (*J-V*) are shown in Fig. 6 and corresponding detailed device photovoltaic parameters are listed in Table 3. In between the carboxylated 1,3-indanedione dyes, **BPhe-ind** dye has shown high efficiency in the absence of co-adsorbents of 2.49% with J_{sc} = 7.33 mA. cm^{-2}, V_{oc} = 0.47 V, FF = 0.72 than MPhe-ind of 1.88% with J_{sc} = 5.57 mA. cm^{-2}, V_{oc} = 0.46 V, FF = 0.73. The high photovoltaic conversion efficiency (PCE) of **BPhe-ind** dye was attributed to the high J_{sc}, which was ascribed to the high light harvesting nature of the **BPhe-ind** dye. These carboxylated 1,3-indanedione dyes were further evaluated with co-adsorbents (CDCA and PA) in order to understand the aggregation phenomena. When **MPhe-ind** and **BPhe-ind** were dyes evaluated with PA the efficiency increased to 2.67% and 2.10% respectively, whereas with CDCA the efficiency is 2.58% and 1.95%. The PA has shown significant influence on improving the device efficiency of carboxylated 1,3-indanedione based dyes over CDCA. These results instigated us to investigate the reason. According to the theoretical studies, the carboxylated 1,3-indanedione dyes were anchored on the TiO_2 in a linear manner, so small size molecules easily reach the gaps of carboxylated 1,3-indanedione dyes on TiO_2. In the comparison of PA and CDCA, PA is small in size, so it can easily take place between the gaps of carboxylated 1,3-indanedione dyes, as a result, it shows high efficiency. In spite of having superior absorption and

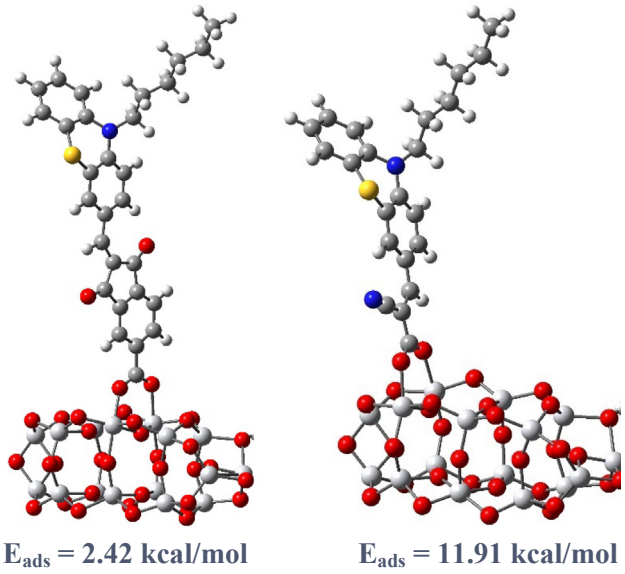

Fig. 5. Adsorption of **MPhe-ind** (left) and **MPhe-cn** (right) on $(TiO_2)_{16}$ cluster.

Table 2
Simulated optical properties of **MPhe-ind** and **BPhe-ind** obtained at PBE0/6-31G(d) level of theory.

Dye	Transition	λ_{cal} (nm)	Oscillator strength	CI coefficient	Dominant contribution (%)
MPhe-ind	$S_0 \rightarrow S_1$	514	0.5549	0.70052	HOMO → LUMO (98)
	$S_0 \rightarrow S_2$	433	0.0441	0.69628	HOMO → L+1 (97)
	$S_0 \rightarrow S_3$	394	0.0028	0.63801	H-3 → LUMO (81)
	$S_0 \rightarrow S_4$	374	0.4629	0.67815	H-1 → LUMO (92)
	$S_0 \rightarrow S_5$	362	0.0010	0.62222	H-3 → L+1 (77)
BPhe-ind	$S_0 \rightarrow S_1$	536	0.6647	0.69383	HOMO → L+1 (98)
	$S_0 \rightarrow S_2$	515	0.4576	0.69048	H-1 → LUMO (95)
	$S_0 \rightarrow S_3$	485	0.0020	0.69673	HOMO → LUMO (97)
	$S_0 \rightarrow S_4$	466	0.0040	0.69707	HOMO → L+2 (97)
	$S_0 \rightarrow S_5$	453	0.0001	0.70495	H-1 → L+2 (97)

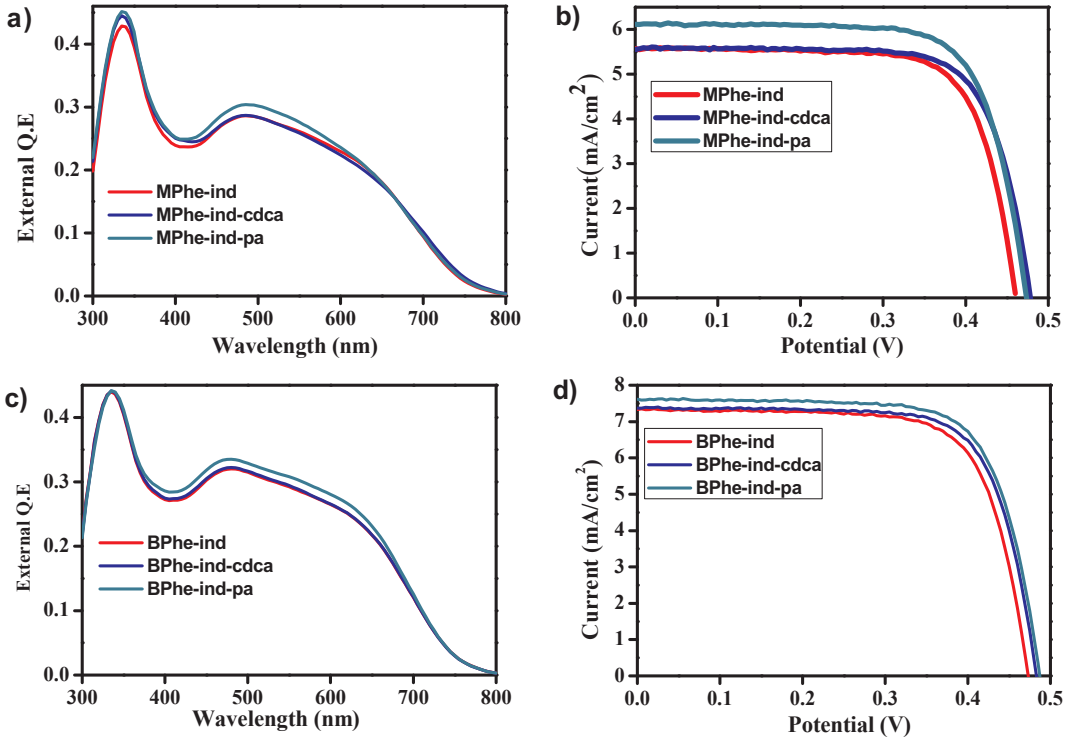

Fig. 6. (**a**) and (**b**) are the IPCE and J-V curves of DSSCs based on **MPhe-ind** dye, (**c**) and (**d**) are the IPCE and *J-V* curves of DSSCs based on **BPhe-ind** dye.

Table 3
DSSCs device performance data of carboxylated 1,3-indanedione and cyanoacetic acid dyes.

Sensitizer	J_{sc}[a] (mA cm^{-2})	V_{oc}[b] (V)	FF[c] (%)	CE[d] (%)
MPhe-ind	5.57	0.460	0.73	1.88
MPhe-ind-CDCA	5.55	0.477	0.73	1.95
MPhe-ind-PA	6.12	0.473	0.72	2.10
BPhe-ind	7.33	0.472	0.72	2.49
BPhe-ind-CDCA	7.37	0.482	0.72	2.58
BPhe-ind-PA	7.61	0.486	0.72	2.67
MPhe-cn	10.16	0.558	0.71	4.07
MPhe-cn-CDCA	9.06	0.596	0.71	3.90
MPhe-cn-PA	9.01	0.564	0.72	3.71
BPhe-cn	10.92	0.543	0.71	4.23
BPhe-cn-CDCA	10.79	0.541	0.71	4.15
BPhe-cn-PA	10.86	0.544	0.71	4.19

The average values of three devices are reported in parenthesis.
[a] Current density.
[b] Open-circuit voltage.
[c] Fill factor.
[d] Photovoltaic conversion efficiency.

electrochemical properties, the carboxylated 1,3-indanedione dyes have shown low efficiency than cyanoacetic acid dyes. The low J_{sc} and unfavorable distribution of LUMO over carboxylated 1,3-indanedione group (Fig. 3) signify the low electron injection into the conduction band of TiO_2. It might be because of competitive conjugation between the carbonyl group and carboxylic acid in carboxylated 1,3-indanedione. The same results can be observed from DFT studies that LUMO distribution on carboxylic anchoring group is 5.6% (Fig. 2) for carboxylated 1,3-indanedione dyes whereas for cyanoacetic acid is 14.5% (Fig. S4). The results indicate that the carbonyl groups presented on carboxylated 1,3-indanedione group retract the electron injection efficiency as a result J_{sc} and overall efficiency decreases.

The incident photon to current conversion efficiency (IPCE) curves of carboxylated 1,3-indanedione dyes showed a similar pattern and extended up to 800 nm, while cyanoacetic acid dyes (MPhe-cn and BPhe-cn) showed up to 660 and 680 nm respectively. The IPCE intensity of **MPhe-ind** and with CDCA was 28% at ~490 nm, but with PA the IPCE intensity was improved to 30%. In the case of **BPhe-ind** sensitizer, the IPCE intensity was 32% with and without CDCA, while with PA it was improved to 33%. Improved IPCE of **BPhe-ind** over **MPhe-ind** were attributed to the increased molar extinction coefficient (ε) of **BPhe-ind** as shown in absorption spectra. In IPCE comparison of carboxylated 1,3-indanedione dyes with CDCA or PA, the carboxylated 1,3-indanedione dyes with PA have shown higher intensity over CDCA, it might be because of decreased dye aggregation.

3.4. Electrochemical impedance spectroscopy

The electrochemical impedance spectroscopy (EIS) of carboxylated 1,3-indanedione and cyanoacetic acid dyes were measured under the dark condition and the Nyquist plots were presented in Fig. 7. All these dyes have shown three semicircles. In general, the first semicircle indicates the charge transfer resistance at the counter electrode and the electrolyte interface [41]. The larger semicircle in the mid-frequency

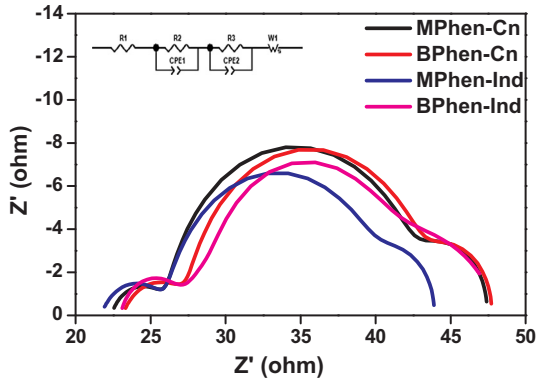

Fig. 7. Electrochemical impedance spectra carboxylated 1,3-indanedione and cyanoacetic acid dyes under dark conditions.

Table 4
EIS analysis of DSSC under dark condition.

Sample	R1	R2	R3
Mphen-cn	22.37	3.73	15.71
Bphen-cn	23.14	4.41	14.78
Mphen-ind	22.92	4.34	13.41
Bphen-ind	22.85	4.99	13.94

region represents the recombination resistance (R3) at the TiO_2/dye/electrolyte interface. The third semicircle in the low-frequency range represents the Warburg diffusion process of I^-/I_3^- in the electrolyte. The data corresponding to the Fig. 7 was depicted in Table 4, where R1 is the series resistance, R2 is the resistance of electron transport in the counter and R3 is the charge recombination resistance at TiO_2/dye/electrolyte interfaces. In the dark impedance analysis, the recombination resistance values of **MPhe-cn**, **BPhe-cn**, **MPhe-ind** and **BPhe-ind** dyes are 15.71, 14.78, 13.94 and 13.41 Ω were obtained, respectively. low recombination resistance might be responsible for low V_{oc} of carboxylated 1,3-indanedione than cyanoacetic acid dyes. On the other hand, among the mono (**MPhe-cn** and **MPhe-ind**) and bis (**BPhe-cn** and **BPhe-ind**) phenothiazine dyes high R3 values are found for bis phenothiazine dyes, which suggest that the double branched molecular engineering is beneficial for restricting the electron recombination.

4. Conclusions

In summary, the replacement of cyanoacetic acid anchoring groups with carboxylated 1,3-indanedione anchoring group resulted in 100 nm enhanced absorption curve with higher molar absorption coefficient and IPCE have been extended up to 800 nm. This is due to high acceptance nature and extended conjugation of carboxylated 1,3-indanedione anchoring group over cyanoacetic acid. In spite of these superior absorption properties, the dyes have shown lower efficiency than cyanoacetic acid dyes. The DFT studies have revealed that the unfavorable LUMO localization over the carboxylated 1,3-indanedione group (i.e. 5.6 and 5.3%) is responsible for low DSSC efficiencies than cyanoacetic acid dyes (14.6 and 14.5%). The observed low LUMO localization on carboxylated 1,3-indanedione group might be because of competitive conjugation between the two carbonyls groups. It diminishes the extent of electron transfer towards carboxylic acid as a result of which J_{sc} and efficiency decreases. The DSSC device efficiency of theses synthesized dyes were not increased much even after the addition of co-adsorbents (CDCA and PA) indicating that these dyes are not aggregating. Further, structural modifications on carboxylated 1,3-indanedione in order to enhance the photovoltaic conversion efficiency by complete utilization of its high light harvesting property are underway.

Acknowledgments

This work was supported by the Korea Institute of Energy Technology Evaluation and Planning (KETEP) and the Ministry of Trade, Industry & Energy (MOTIE) of the Republic of Korea (No. 20163010012310). The Human resources program in energy technology of the KETEP, granted from the MOTIE, Republic of Korea (No. 20174030201760). Fundamental R&D program for Core Technology of Materials (10050966) funded by the Knowledge Economy, Republic of Korea.

Appendix A. Supplementary material

Supplementary data to this article can be found online at https://doi.org/10.1016/j.cplett.2018.11.026.

References

[1] B.E. Hardin, H.J. Snaith, M.D. McGehee, Nat. Photon. 6 (2012) 162–169.
[2] S. Zhang, X. Yang, Y. Numata, L. Han, Energy Environ. Sci. 6 (2013) 1443–1464.
[3] Y. Wu, W. Zhu, Chem. Soc. Rev. 42 (2013) 2039–2058.
[4] B. O'Regan, M. Gratzel, Nature 353 (1991) 737–740.
[5] L. Zhang, M.J. Cole, J. Mater. Chem. A 5 (2017) 19541–19559.
[6] P. naik, R. Su, D.D. Babu, A. Ei-Shafei, A.V. adhkari, J. Iran. Chem. Soc. 14 (2017) 2457–2466.
[7] A. Yella, H.W. Lee, H.N. Tsao, C. Yi, A.K. Chandiran, M.K. Nazeeruddin, E.W.G. Diau, C.Y. Yeh, M. ZakeeruddinS, M. Grätzel, Science 334 (2011) 629–634.
[8] H. Song, W. Tang, S. Zhao, Q. Liu, Y. Xie, Dyes Pigments 155 (2018) 323–331.
[9] L. Han, A. Islam, H. Chen, C. Malapaka, B. Chiranjeevi, S.X. Zhang, M. Yang Yanagida, High efficiency dye-sensitized solar cell with a novel co-adsorbent, Energy Environ. Sci. 5 (2012) 6057–6060.
[10] T.-D. Nguyen, Y.-P. Lan, C.-G. Wu, Inorg. Chem. 57 (2018) 1527–1534.
[11] K. Ganesh, B. Vinayak, T. Suresh, G. Wu, J. Li, X. Fang, F. Kong, S. Dai, S. Niveditha, K. Bhanuprakash, M. Chandrasekharam, Dalton Trans. 43 (2014) 14992–15003.
[12] Z. Ning, Y. Fu, H. Tian, Energy Environ. Sci. 3 (2010) 1170–1181.
[13] Y.Z. Wu, M. Marszalek, S.M. Zakeeruddin, Q. Zhang, H. Tian, M. Grätzel, W.H. Zhu, Energy Environ. Sci. 5 (2012) 8261–8272.
[14] J.H. Yum, T.W. Holcombe, Y. Kim, K. Rakstys, T. Moehl, J. Teuscher, J.H. Delcamp, M.K. Nazeeruddin, M. Grätzel, Sci. Rep. 3 (2013) 2446.
[15] X.F. Zang, Z.S. Huang, H.L. Wu, Z. Iqbal, L.Y. Wang, H. Meier, D. Cao, J. Power Sources 271 (2014) 455–464.
[16] D.D. Babu, D. Elsherbiny, H. Cheema, A. El-Shafei, A.V. Adhikari, Dyes Pigments 132 (2016) 316–328.
[17] S. Mathew, A. Yella, P. Gao, R. Humphry-Baker, F.E. Curchod Basile, N. Ashari-Astani, I. Tavernelli, U. Rothlisberger, M.K. Nazeeruddin, M. Grätzel, Nat. Chem. 6 (2014) 242–247.
[18] A. Mishra, M.K.R. Fischer, P. Bäuerle, Angew. Chem. Int. Ed. 48 (2009) 2474–2499.
[19] K. Kakiage, et al., Chem. Commun. 51 (2015) 15894.
[20] X. Liao, H. Zhang, J. Huang, G. Wu, X. Yin, Y. Hong, Dyes Pigments 158 (2018) 240–248.
[21] H. Cheng, Y. Wu, J. Su, Z. Wang, G.R. Prasad, M. Liang, Z. Sun, S. Xue, Dyes Pigments 149 (2018) 16–24.
[22] D. Cao, J. Peng, Y. Hong, X. Fang, L. Wang, H. Meier, Org. Lett. 13 (2011) 1610–1613.
[23] Y.H. Lee, R.K. Chitumalla, B.Y. Jang, H.R. Jang, J.T. Suresh, J.H. Kim, Dyes Pigments 133 (2016) 161–172.
[24] J.H. Park, B.Y. Jang, T. Suresh, J.-H. Ryu, S.-H. Kim, Y.-A. Son, J.H. Kim, Synthetic Metals 203 (2015) 235–242.
[25] J.N. Clifford, E.M. Ferrero, A. Viterisi, E. Palomares, Chem. Soc. Rev 40 (2011) 1635–1646.
[26] W.-C. Chen, S. Nachimuthu, J.-C. Jiang, Sci. Rep. 7 (2017) 4979.
[27] Z.-S. Huang, H. Meier, D. Ca, J. Mater. Chem. C 4 (2016) 2404–2426.
[28] J.-S. Luo, Z.-Q. Wan, C.-Y. Jia, Chin. Chem. Lett. 27 (2016) 1304–1318.
[29] N. Shibayama, Y. Inoue, M. Abe, S. Kajiyama, H. Ozawa, H. Miura, H. Arakawa, Chem. Commun. 51 (2015) 12795–12798.
[30] K. Sayama, S. Tsukagoshi, K. Hara, Y. Ohga, A. Shinpou, Y. Abe, S. Suga, H. Arakawa, J. Phys. Chem. B 106 (2002) 1363–1371.
[31] K. Ganesh, Ch.P. Kumar, P. Salvatori, G. Marotta, M.L. Gräzia, O. Bizzarri, F.D. Angelis, M. Chandrasekharam, Inorgan. Chim. Acta 442 (2016) 158–166.
[32] M.J. Frisch, G.W. Trucks, H.B. Schlegel, G.E. Scuseria, J. Cioslowski, D.J. Fox, et al. Wallingford CT, 2009.
[33] A.D. Becke, J. Chem. Phys. 98 (1993) 5648.
[34] A.D. Becke, Density-functional thermochemistry. IV. A new dynamical correlation functional and implications for exact-exchange mixing, J. Chem. Phys. 104 (1996) 1040–1046.
[35] C. Lee, W. Yang, R.G. Parr, Phys. Rev. B Condens. Matter 37 (1988) 785–789.
[36] J.P. Perdew, K. Burke, M. Ernzerhof, Phys. Rev. Lett. 77 (1996) 3865–3868.
[37] C. Adamo, V. Barone, J. Chem. Phys. 110 (1999) 6158–6170.
[38] S. Miertus, E. Scrocco, J. Tomasi, J. Chem. Phys. 55 (1981) 117–129.
[39] M. Cossi, V. Barone, R. Cammi, J. Tomasi, Chem. Phys. Lett. 255 (1996) 327–335.
[40] P. Persson, J.C.M. Gebhardt, S. Lunell, J. Phys. Chem. B 107 (2003) 3336–3339.
[41] F.-S. Francisco, B. Juan, G.-B. Germa', B. Gerrit, H. Anders, Solar Energy Mater. Solar Cells 87 (2005) 117–131.